liquid resistance in both horizontal and vertical wicks and the increased vapor resistance leads to an optimum top and bottom wick thickness, as shown in Fig. 2. Figure 2 also shows that the maximum heat transfer decreases monotonically with increasing the top and bottom wick shape parameter $\gamma_w = \sqrt{\varepsilon_w/K_w}$. Based on the investigation of flow through porous media by Vafai and Tien,[6] an increase of γ_w leads to a larger flow resistance in the wick, and thus, to a lower maximum heat transfer.

Figure 3 shows the effects of vertical wick structure on the maximum heat transfer capacity. An optimum vertical wick thickness exists for any given porous media shape parameter of the vertical wick $\gamma_{vw} = \sqrt{\varepsilon_{vw}/K_{vw}}$. A large vertical wick thickness leads to a large flow rate of liquid from the bottom wick to the top wick, and thus, to a higher maximum heat transfer. On the other hand, a large vertical wick thickness produces a larger resistance to the vapor flow due to the decrease of the vapor space, thus decreasing the maximum heat transfer. The balance of these two effects leads to an optimum vertical wick thickness for the maximum heat transfer capacity. Figure 3 also shows that for any given vertical wick thickness an optimum vertical wick shape parameter is observed. The optimum value occurs due to the influence of the vertical wick material on both the frictional resistance to the liquid flow within the vertical wicks and the capillary force of the vertical wicks. A large vertical wick shape parameter increases the frictional resistance to the liquid flow in the vertical wicks, thus decreasing the flow rate of liquid from the bottom wick to the top wick. Conversely, a large vertical wick shape parameter increases the capillary force of the vertical wicks, thus increasing the liquid flow rate in the vertical wicks. The internal balance of these two effects leads to the optimum vertical wick shape parameter.

Optimization of the Heat Pipe Design

To simplify the optimization of the disk-shaped heat pipe design, the Darcy number is used to reflect the effects of the wick structure (both the wick thickness and the porous wick shape parameter), as shown in Fig. 4. Therefore, the maximum heat transfer capacity of the disk-shaped heat pipe is a function of the internal flow channel angle, the Darcy number of the top and bottom wicks, and the Darcy number of the vertical wick. Figures 1 and 4 are then used to optimize the disk-shaped heat pipe design.

It should be mentioned that the use of Fig. 4 requires a judicious use of the parameters. As shown in Fig. 4, an optimum Da_w exists for the heat pipe design. Different wick material and thickness can be selected to obtain this optimum value of Da_w. Since $Da_w = 1/(\gamma_w h_w)^2$, and the maximum heat transfer capacity increases dramatically as γ_w decreases, it is preferred to select a smaller γ_w and a larger h_w to obtain a better result. However, from the boiling limitation considerations, a smaller γ_w or a larger h_w results in an increased thermal resistance to the heat transfer across the liquid-saturated wick, thus decreasing the maximum vertical heat flux of the disk-shaped heat pipe. Therefore, the boiling limitation should be taken into consideration when selecting wick material and thickness.

Conclusions

A pseudo-three-dimensional analytical model has been formulated for the parametric study of the maximum heat transfer capacity of a disk-shaped heat pipe. The maximum heat transfer capacity was evaluated as a function of design parameters based on the capillary limitation. The results show that, for a fixed heat pipe thickness, the optimized flow channel angle, top and bottom wick thickness, vertical wick thickness, and shape parameter of the vertical wicks exist for which the capillary limit of the disk-shaped heat pipe reaches a maximum value. An optimized disk-shaped heat pipe design was obtained based on the parametric study and the boiling limitation.

Acknowledgments

This work was supported by the Department of Energy under Contract DE-FGO2-93ER61612. The authors would like to thank Thomas Blue for his help on this work.

References

[1]Vafai, K., Zhu, N., and Wang, W., "Analysis of Asymmetrical Disk-shaped and Flat Plate Heat Pipes," *Journal of Heat Transfer*, Vol. 117, No. 1, 1995, pp. 209–218.

[2]Zhu, N., and Vafai, K., "The Effects of Liquid-Vapor Coupling and Non-Darcian Transport on Asymmetrical Disk-Shaped Heat Pipes," *International Journal of Heat and Mass Transfer* (to be published).

[3]Vafai, K., "Convective Flow and Heat Transfer in Variable Porosity Media," *Journal of Fluid Mechanics*, Vol. 147, 1984, pp. 233–259.

[4]Chi, S. W., *Heat Pipe Theory and Practice*, Hemisphere, New York, 1976.

[5]Dunn, P. D., and Reay, D. A., *Heat Pipes*, 3rd ed., Pergamon, New York, 1982.

[6]Vafai, K., and Tien, C. L., "Boundary and Inertia Effects on Flow and Heat Transfer in Porous Media," *International Journal of Heat and Mass Transfer*, Vol. 24, No. 2, 1981, pp. 195–203.

Direct Least-Square Solutions to Integral Equations Containing Discrete Data

J. I. Frankel*
University of Tennessee, Knoxville, Tennessee 37996-2210

Introduction

MATHEMATICAL models in engineering and physics often contain noisy discrete data. Yet it is often desired to obtain a solution to either a differential or integral equation in the presence of such data. Shih et al.[1] encountered such a situation where an experiment was devised to map the intensity of thermal radiation leaving a diffuse hemispherical shell. Shih et al. developed a simplified mathematical model that was expressed in terms of a Fredholm integral equation of the second kind. Interestingly enough, this equation permits an exact solution. In this case, the radiosity distribution along the surface of the hemisphere is expressible in terms of an integral containing the surface temperature distribution raised to the fourth power.

Instrumental to the success of that study was the availability of the exact solution for the radiosity distribution. Unfortunately, most situations preclude the determination of the exact solution for an integral equation that is derived from radiative heat transfer. In response to this dilemma, this Note revisits the exposition of Shih et al. and presents a general method for determining the unknown radiosity in the presence of noisy discrete temperature data based solely on knowledge of the

Received April 26, 1995; revision received June 30, 1995; accepted for publication Aug. 10, 1995. Copyright © 1995 by the American Institute of Aeronautics and Astronautics, Inc. All rights reserved.

*Associate Professor, Mechanical and Aerospace Engineering Department. Member AIAA.

integral equation describing the radiosity. The procedure offered here can be extended to other problems in heat and mass transfer, but is developed in the context of the problem considered by Shih et al.

Problem Statement and the Exact Solution

The radiosity distribution along the diffuse interior surface, as described in Shih et al.,[1] is obtained by solving a Fredholm integral equation of the second kind.[2] In the dimensionless form, the formulation offered by Shih et al. can be written as

$$Q_0(\eta) = f(\eta) + \beta \int_{\xi=0}^{1} Q_0(\xi)\sin(\alpha\xi)\, d\xi, \qquad \eta \in [0, 1] \tag{1a}$$

with

$$f(\eta) = \varepsilon\theta^4(\eta) + \lambda \tag{1b}$$

and where the following dimensionless functions and quantities are used:

$$\bar{Q}_0(x) = R(x)/\sigma T_a^4 \tag{2a}$$

$$\bar{\theta}(x) = T(x)/T_a \tag{2b}$$

$$x = \alpha\eta, \qquad \eta \in [0, 1] \tag{2c}$$

$$y = \alpha\xi, \qquad \xi \in [0, 1] \tag{2d}$$

$$\alpha = \pi/2 \tag{2e}$$

$$\lambda = (\rho/2) < 1 \tag{2f}$$

$$\beta = \lambda\alpha \tag{2g}$$

For simplicity in the mathematical notation, the dependent variables used in Eq. (1) are defined by

$$Q_0(\eta) = \bar{Q}_0(\alpha\eta) \tag{3a}$$

$$\theta(\eta) = \bar{\theta}(\alpha\eta) \tag{3b}$$

Equation (1a) is rather unusual in that it is possible to solve for $Q_0(\eta)$ in an exact manner. Observe that the integral term shown in Eq. (1a) evaluates to the unknown constant

$$c = \int_{\xi=0}^{1} Q_0(\xi)\sin(\alpha\xi)\, d\xi \tag{4}$$

With this definition, the exact solution for Eq. (1a) is

$$Q_0(\eta) = \varepsilon\theta^4(\eta) + \lambda + \frac{\beta}{1-\lambda}\left[\frac{\rho}{\pi} + \varepsilon\int_{\xi=0}^{1} \theta^4(\xi)\sin(\alpha\xi)\, d\xi\right], \qquad \eta \in [0, 1] \tag{5}$$

The exact solution displayed in Eq. (5) was necessary for Shih et al.[1] to arrive at the model solution for the radiosity $Q_0(\eta)$. Shih et al. proposed to curve fit the measured temperature data to arrive at an analytic representation for the temperature. This result is then supplied to Eq. (5) from which the radiosity distribution is recovered. As mentioned earlier, Eq. (1a) is rather unique in engineering analysis since an exact solution can be developed. But suppose that an exact solution could not be found.

Direct Least-Squares Methodology: Residual Minimization

In this section, a direct least-squares method[3] is proposed for approximating the unknown dimensionless radiosity $Q_0(\eta)$ shown in Eq. (1a). The necessary definitions, background, and motivation are presented from which future generalizations can be made. The approach discussed here has its basis from the classical weighted residual method.[4]

To begin, the unknown function shown in Eq. (1a) is expressed as

$$Q_0(\eta) = \sum_{j=0}^{\infty} a_j\psi_j(\eta), \qquad \eta \in [0, 1] \tag{6}$$

Here $\{\psi_j(\eta)\}_{j=0}^{\infty}$ are a linearly independent set of global basis functions having corresponding expansion coefficients $\{a_j\}_{j=0}^{\infty}$. In practical calculations, this series is truncated after a finite number of terms, e.g., $j = N$, thus retaining $N + 1$ terms in the expansion. The approximate solution to $Q_0(\eta)$ is denoted as $Q_0^N(\eta)$ and is given as

$$Q_0(\eta) \approx Q_0^N(\eta) = \sum_{j=0}^{N} a_j^N\psi_j(\eta), \qquad \eta \in [0, 1] \tag{7}$$

where we note, in general, that $a_j \approx a_j^N$ for sufficiently large N. For demonstration, a monomial set $\psi_j(\eta) = \eta^j$, $j = 0, 1, \ldots, N$, $\eta \in [0, 1]$ is used, but, in general, it is advisable to use an orthogonal set of basis functions[5] owing to ill-conditioning effects.

Substituting the approximate solution $Q_0^N(\eta)$ described by Eq. (7) into Eq. (1a) produces

$$R_N(Q_0^N(\eta)) = Q_0^N(\eta) - f(\eta) - \beta\int_{\xi=0}^{1} Q_0^N(\xi)\sin(\alpha\xi)\, d\xi, \qquad \eta \in [0, 1] \tag{8}$$

Here, $R_N(Q_0^N(\eta))$ represents the residual function that must be introduced to maintain the equal sign shown in Eq. (8). If $Q_0(\eta) = Q_0^N(\eta)$, then $R_N(Q_0(\eta)) = 0$. In other words, unless the true solution is a linear combination of the chosen basis functions, no set of expansion coefficients $\{a_j^N\}_{j=0}^N$ can make the residual function $R_N(Q_0^N(\eta))$ vanish for all η in the closed interval. However, suitable expansion coefficients can be obtained by making the residual function small in some sense.

Before proceeding further some additional mathematical definitions in the context of the weighted residual method need to be presented. A systematic way of arriving at a suitable set of expansion coefficients in a manner consistent with making $R_N(Q_0^N(\eta))$ small in some sense is to require[4]

$$\langle R_N(Q_0^N(\eta)), \Psi_k(\eta)\rangle_{w_k(\eta)} = 0, \qquad k = 0, 1, \ldots, N, \qquad \eta \in [0, 1] \tag{9a}$$

which states that the residual function $R_N(Q_0^N(\eta))$ is orthogonal to the test function $\Psi_k(\eta)$ with respect to the weight function $w_k(\eta)$. Here, the inner product follows the conventional definition[5]

$$\langle R_N(Q_0^N(\eta)), \Psi_k(\eta)\rangle_{w_k(\eta)} = \int_{\eta=0}^{1} w_k(\eta)R_N(Q_0^N(\eta))\Psi_k(\eta)\, d\eta, \qquad k = 0, 1, \ldots, N \tag{9b}$$

For motivational purposes, the derivation of the continuous least-squares method is presented based on the direct minimization of the L_2 – norm.[6] The L_2 – norm of the residual function is defined as

$$S(\{a_j^N\}_{j=0}^N) = \|R_N(Q_0^N(\eta))\|_2^2 = \langle R_N(Q_0^N(\eta)), R_N(Q_0^N(\eta))\rangle_1 = \int_{\eta=0}^{1} R_N^2(Q_0^N(\eta))\, d\eta \tag{9c}$$

Therefore, to determine the unknown expansion coefficients by this method, we minimize the integral shown in Eq. (9c) with respect to each unknown expansion coefficient, namely,

$$\frac{\partial S}{\partial a_k^N} = \frac{\partial \|R_N(Q_0^N(\eta))\|_2^2}{\partial a_k^N} = 2\int_{\eta=0}^{1} \frac{\partial R_N(Q_0^N(\eta))}{\partial a_k^N} R_N(Q_0^N(\eta))\, d\eta = 0 \tag{10}$$

for $k = 0, 1, \ldots, N$. This concept can be generalized to account for discrete data in the model.

Substituting the explicit expansion for $Q_0^N(\eta)$ shown in Eq. (7) into Eq. (8) produces

$$R_N(Q_0^N(\eta)) = -f(\eta) + \sum_{j=0}^{N} a_j^N(\eta^j - \beta C_j), \qquad \eta \in (0, 1) \tag{11a}$$

where

$$C_j = \int_{\xi=0}^{1} \xi^j \sin(\alpha\xi)\, d\xi, \qquad j = 0, 1, \ldots, N \tag{11b}$$

Suppose that the surface temperature $\theta(\eta)$ is measured at M discrete angles η, i.e., η_i, $i = 1, 2, \ldots, M$, such that $\eta_i \in [0, 1]$. Let us denote these measured values for the temperature as $\theta_i = \theta(\eta_i)$, $i = 1, 2, \ldots, M$. For example, consider the 21-point data sets tabulated in Table 1. The second data set displayed in Table 1 indicates the existence of scatter in the collected data. With this in mind, Eq. (11a) is evaluated at $\eta = \eta_i$, $i = 1, 2, \ldots, M$ to arrive at the discrete residuals

$$R_N(Q_0^N(\eta_i)) = -f(\eta_i) + \sum_{j=0}^{N} a_j^N(\eta_i^j - \beta C_j) \qquad i = 1, 2, \ldots, M \tag{12}$$

In an analogous manner as previously described for the continuous least-squares method, we now form the L_2 − norm of the discrete $R_N(Q_0^N(\eta_i))$ for $i = 1, 2, \ldots, M$. Doing so produces

$$S(\{a_j^N\}_{j=0}^N) = \|R_N\|_2^2 = \sum_{i=1}^{M} \left[-f(\eta_i) + \sum_{j=0}^{N} a_j^N(\eta_i^j - \beta C_j) \right]^2 \tag{13}$$

The unknown expansion coefficients $\{a_j^N\}_{j=0}^N$ are chosen by minimizing $S(\{a_j^N\}_{j=0}^N)$ with respect to each unknown expansion coefficient, i.e.,

$$\frac{\partial S}{\partial a_k^N} = 0, \qquad k = 0, 1, \ldots, N \tag{14}$$

Performing the indicated partial differentiation on Eq. (13) and equating the result to zero produces

$$\sum_{j=0}^{N} a_j^N \left[\sum_{i=1}^{M} (\eta_i^j - \beta C_j)(\eta_i^k - \beta C_k) \right] = \sum_{i=1}^{M} f(\eta_i)(\eta_i^k - \beta C_k), \qquad k = 0, 1, \ldots, N \tag{15}$$

which is of the form $A\bar{x} = \bar{b}$. Once the expansion coefficients are resolved through the solution of a system of $(N + 1)$ linear equations, the dimensionless radiosity $Q_0^N(\eta)$ can be reconstructed through Eq. (7). The condition number, which is often used as an indicator of ill conditioning,[7] increases as with increasing values of N. The use of an orthogonal basis, such as Chebyshev polynomials in the interval $[-1, 1]$, substantially reduces the ill-conditioning effect. Next, some comparative results are presented, illustrating the effectiveness of this approach.

Table 1 Discrete data sets for θ_i, $i = 1, 2, \ldots, M = 21$, $\varepsilon = 0.9$, $\hat{\theta}_0 = 0.8$, and $\hat{\theta}_1 = 0.1$

	Data set 1, $\omega = 0$	Data set 2, $\omega = 0.05$
η_i	θ_i	θ_i
0	0.8	0.775413
0.05	0.794925	0.793736
0.1	0.7804	0.73125
0.15	0.757475	0.761414
0.2	0.7272	0.756074
0.25	0.690625	0.663781
0.3	0.6488	0.654975
0.35	0.602775	0.631161
0.4	0.5536	0.525486
0.45	0.502325	0.499201
0.5	0.45	0.455372
0.55	0.397675	0.414666
0.6	0.3464	0.318653
0.65	0.297225	0.312849
0.7	0.2512	0.212673
0.75	0.209375	0.163927
0.8	0.1728	0.151002
0.85	0.142525	0.12596
0.9	0.1196	0.0726753
0.95	0.105075	0.141372
1	0.1	0.0970176

Results

In this section, a comparison of results is presented indicating the merit for the proposed methodology. The symbolic manipulation software package Mathematica™ (Ref. 8) was used to perform all the analytic, numeric, and graphic computations presented here. The discrete temperature data presented in Table 1 was generated using

$$\theta_i = \hat{\theta}_p(\eta_i) + \omega Rand(i), \qquad i = 1, 2, \ldots, M \tag{16a}$$

where $\omega \in [0, 1]$, $M = 21$, and $Rand(i)$ is a randomly generated number in the interval $[-1, 1]$, and where $\hat{\theta}_p(\eta)$ is given by

$$\hat{\theta}_p(\eta) = \hat{\theta}_0 + (\hat{\theta}_0 - \hat{\theta}_1)(-3\eta^2 + 2\eta^3), \qquad \eta \in [0, 1] \tag{16b}$$

Fewer data points can be used, but some care must be observed when using the least-squares method in the presence of a limited amount of data.[7]

An exact solution for the radiosity $Q_0(\eta)$ when $\omega = 0$ can be established from Eq. (1a). For the calculations presented in this work, let $\hat{\theta}_0 = 0.8$, $\hat{\theta}_1 = 0.1$, and $\varepsilon = 0.9$. A contrast between the method of Shih et al.[1] and the present methodology is now discussed.

Initial attention is directed toward the errorless data set (data set 1) shown in Table 1. The procedure proposed by Shih et al. requires knowledge of the exact solution for the mathematical model. Thus, a least-squares curve fit to the data displayed in Table 1 is performed from which an analytic representation for $\theta_N(\eta)$ is obtained. Figure 1a presents the dimensionless radiosity distribution for the exact solution when $\omega = 0$ and the generated solution $Q_0^N(\eta)$ when $N = 3$ as calculated from Eq. (5). Figure 1b graphically displays the

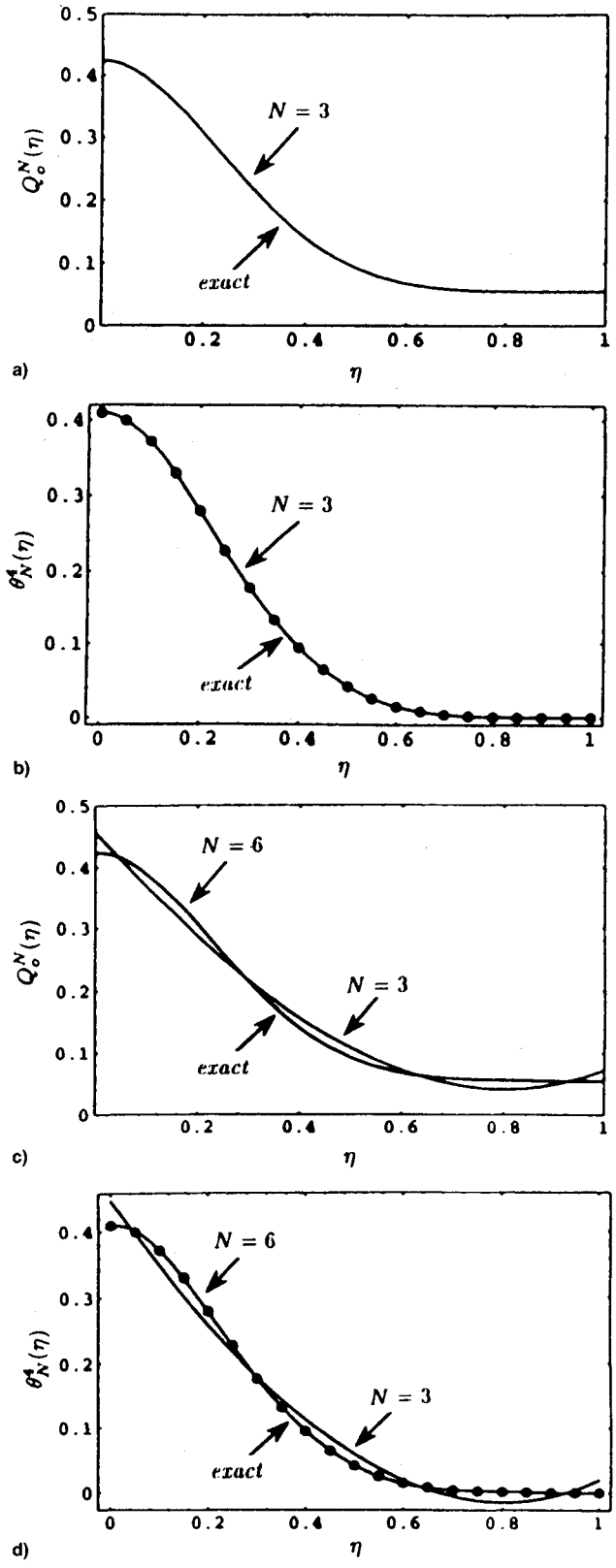

Fig. 1 Radiosity $Q_o^N(\eta)$ and temperature $\theta_N^4(\eta)$ distributions using the method of Shih et al.[1] and the present approach in the presence of the errorless data set ($\omega = 0$) shown in Table 1.

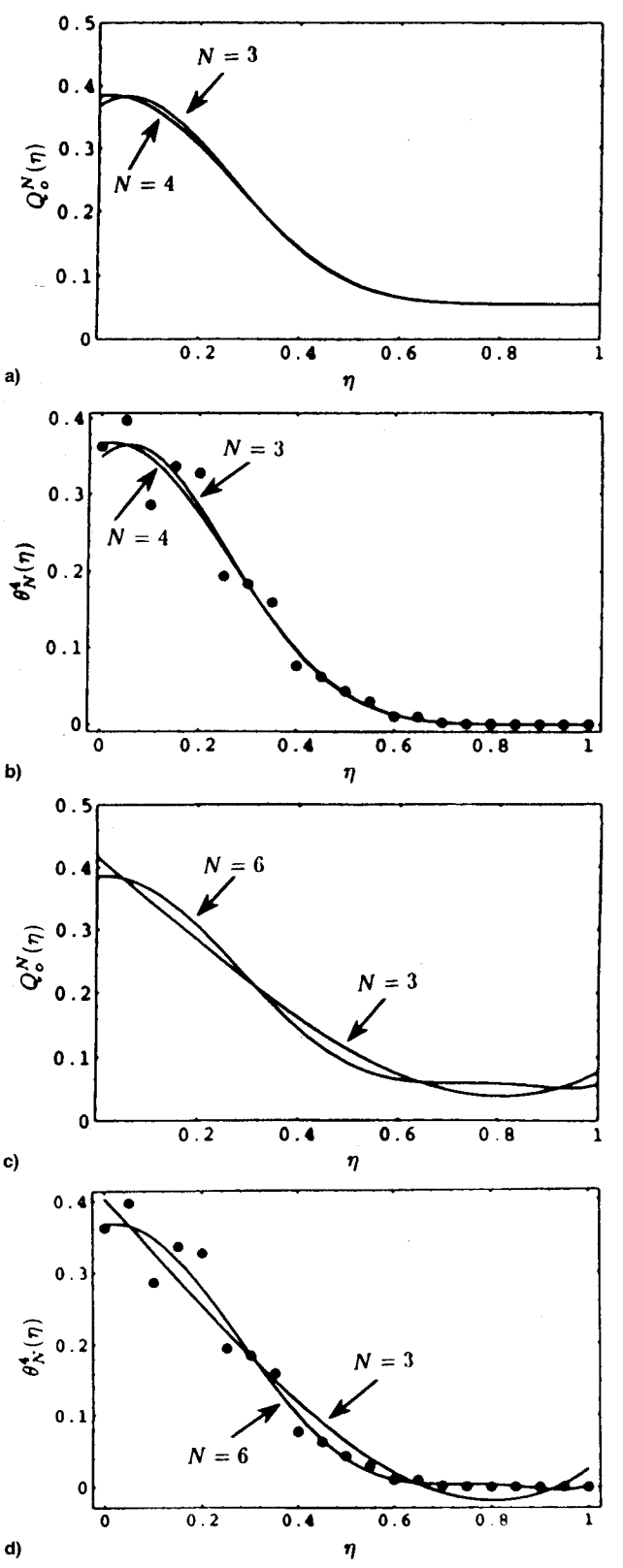

Fig. 2 Radiosity $Q_o^N(\eta)$ and temperature $\theta_N^4(\eta)$ distributions using the method of Shih et al.[1] and the present approach in the presence of the noisy data set ($\omega = 0.05$) shown in Table 1.

discrete data as generated from Eq. (16a) for θ_i raised to the fourth power, the exact solution for $\theta^4(\eta)$ and $\theta_N^4(\eta)$ when $N = 3$ and $\omega = 0$.

Figure 1c presents the dimensionless radiosity distribution when $N = 3, 6$ as obtained using the method proposed in this article. Again the exact reference solution is presented. To locate the optimum choice[7] for N it is necessary to reconsider the initial set of temperature data. Thus, an analytic expression for $\theta_N^4(\eta)$ from Eq. (1a) is required to investigate the variance. This procedure is still under investigation and warrants further theoretical considerations. Finally, Fig. 1d presents $\theta_N^4(\eta)$ as obtained from Eq. (1a).

Figure 2 presents a similar set of plots corresponding to Fig. 1, with the exception that $\omega = 0.05$, which corresponds to the second data set shown in Table 1. Again, the proposed procedure works well, even in the presence of noise. A favorable comparison is evident. The radiosity results when $N = 4$ produced by the method of Shih et al.[1] is shown in Fig. 2a. The radiosity distribution as developed by the proposed method when $N = 6$ is displayed in Fig. 2c. Likewise, the resulting temperature distribution shown in Fig. 2b, when $N = 4$, is clearly in line with the results offered in Fig. 2d when $N = 6$.

To conclude this Note, the proposed methodology possesses merit in situations that do not easily permit the development of an exact solution. This approach deserves more rigorous development and attention.

Acknowledgment

The work presented here was supported by Grant CCR-9320385, provided by the National Science Foundation.

References

[1]Shih, S. H., Love, T. J., and Francis, J. E., "Direct Measurement of the Radiosity of a Nonisothermal Hemispherical Cavity," *Heat Transfer, Thermal Control, and Heat Pipes*, edited by W. B. Olstad, Vol. 70, Progress in Astronautics and Aeronautics, AIAA, New York, 1980, pp. 171–188.

[2]Tricomi, F. G., *Integral Equations*, Dover, New York, 1985.

[3]Linz, P., "The Solution of Volterra Equations of the First Kind in the Presence of Large Uncertainties," *Treatment of Integral Equations by Numerical Methods*, edited by C. T. H. Baker and G. F. Miller, Academic, New York, 1982, pp. 123–130.

[4]Finlayson, B. A., *The Method of Weighted Residuals and Variational Principles*, Academic, New York, 1972.

[5]Frankel, J. I., "Cumulative Variable Formulation to Transient Conductive and Radiative Transport in Participating Media," *Journal of Thermophysics and Heat Transfer*, Vol. 9, No. 2, 1995, pp. 210–218.

[6]Wing, G. M., *A Primer on Integral Equations of the First Kind*, Society for Industrial and Applied Mathematics, Philadelphia, PA, 1991.

[7]Gerald, C. F., and Wheatley, P. O., *Applied Numerical Analysis*, 5th ed., Addison–Wesley, Reading, MA, 1994.

[8]Wolfram, S., *Mathematica*, 2nd ed., Addison–Wesley, Reading, MA, 1992.

Heat Transfer Transients in Stagnation Flows Due to Changes in Flow Velocity

R. A. Brittingham,* E. C. Mladin,* and D. A. Zumbrunnen†
Clemson University, Clemson, South Carolina 29634-0921

Nomenclature

C = steady-state freestream velocity gradient
C_* = constant dimensionless freestream velocity gradient from potential flow theory, Cw/V_i
h = heat transfer coefficient
k = thermal conductivity
Nu_* = ratio of instantaneous Nusselt number to steady-state Nusselt number, Nu_w/Nu_{w0}
t = time
U_∞ = local velocity component parallel to the surface in the freestream
$U_{\infty *}$ = dimensionless freestream velocity, U_∞/V_{i0}
V_i = incident flow velocity
w = characteristic length scale, e.g., jet width or cylinder diameter
x = distance along impingement surface from stagnation line
Γ = dimensionless thermal boundary-layer thickness, $C\Delta^2/\nu$
Λ = dimensionless hydrodynamic boundary-layer thickness, $C\delta^2/\nu$
ν = kinematic viscosity
τ = dimensionless time, Ct

Subscript
0 = pertaining to $t = 0$ and steady-state conditions

Received April 10, 1995; revision received July 21, 1995; accepted for publication July 21, 1995. Copyright © 1995 by the American Institute of Aeronautics and Astronautics, Inc. All rights reserved.

*Research Assistant, Thermal and Fluid Sciences Research Laboratory, Department of Mechanical Engineering.

†Associate Professor, Thermal and Fluid Sciences Research Laboratory, Department of Mechanical Engineering. Member AIAA.

Introduction

CONVECTIVE heat transfer often occurs where flow or surface-related disturbances are intentionally induced or are the result of some change in operating conditions. Such disturbances induce thermal transients in the fluid that propagate within the fluid and cause changes in heat transfer coefficients. Examples of disturbances include pulsations in an impinging jet flow, velocity changes due to incident large-scale flow structures, and changed heat fluxes at a surface. An understanding and quantification of the ensuing thermal transients can be useful in assessing whether available heat transfer correlations can be implemented in developing simple thermal models or in efforts to employ nonlinear dynamical effects to induce changes in time-averaged heat transfer coefficients. Recently, e.g., theoretical models have been developed to disclose over long time intervals nonlinear dynamical effects in stagnation flows.[1,2] With nonlinear dynamical effects included, sinusoidal fluctuations can lead to nonsinusoidal responses in boundary layers, and thereby, reveal conditions where time-averaged heat transfer can be altered.

In this study, a model[2] of instantaneous convective heat transfer in a planar stagnation flow was implemented to determine specifically responses to single ramp-up or ramp-down changes in the incident flow velocity. A primary motivation for this work was the need for documentation of transient effects in a simplified format with the realization that implementation of the recently developed nonlinear dynamical model is difficult in practice. Response times for convective heat transfer coefficients are given in a generalized format to account for dependencies on flow velocities, characteristic dimensions such as nozzle widths or cylinder diameters, and thermophysical properties. Equivalent first-order time constants and transient durations are tabulated for ready use. A systematic presentation of the nonlinear dynamical transients of this study is available in conference proceedings.[3]

Analytical Methods

Complete documentation of the nonlinear dynamical model that is implemented here has been published previously.[2] In summary, a solution methodology was sought that was consistent with approaches used in recent studies of nonlinear dynamics and chaos in thermal or discrete mechanical systems. The responses of such systems are commonly represented by a system of first-order, ordinary differential equations (ODEs). The approach that was selected is related to the von Kármán–Pohlhausen technique,[4] since this technique has been widely used in studies of steady stagnation flows and